

Research Article

Open-Tip Carbon Nanotubes for Enhanced Methane Adsorption Performance: A Comparative Study

Yanyan Feng ^{1,2}, Yanjie Li,¹ Wen Yang ^{1,2}, Di Yang,¹ Guangyuan Ye,¹ and Shufen Zhang^{1,3}

¹Department of Chemistry and Bioengineering, Guilin University of Technology, Guilin 541004, China

²Guangxi Key Laboratory of Electrochemical and Magnetochemical Functional Materials,

Department of Chemistry and Bioengineering, Guilin University of Technology, Guilin 541004, China

³State Key Laboratory of Fine Chemicals, Dalian University of Technology, Dalian 116024, China

Correspondence should be addressed to Wen Yang; yangwen167@163.com

Received 14 August 2018; Revised 6 November 2018; Accepted 8 November 2018; Published 26 November 2018

Academic Editor: Eduard Llobet

Copyright © 2018 Yanyan Feng et al. This is an open access article distributed under the Creative Commons Attribution License, which permits unrestricted use, distribution, and reproduction in any medium, provided the original work is properly cited.

A series of open-tip carbon nanotubes (CNTs) were obtained by HNO₃ modification with various concentrations of as-prepared carbon nanotubes via the CVD method, and this work aimed at investigating the structural features of open-tip CNTs for the methane capability. Modified CNTs had higher specific surface area and larger total pore volume, and importantly, greater micropore volume was obtained through HNO₃ modification of the as-prepared CNTs. The remarkably high methane adsorption capacities were measured on the modified CNTs under pressure ranges of 0~4.0 MPa at 298 K. The resulted H-CNT, which exhibited highest specific surface area and micropore volume, showed high methane uptake of 26.15 mg/g from the D-A model. This value was nearly as twice as the methane uptake of original CNTs (13.62 mg/g), along with an initial adsorption heat of 19.4 kJ/mol at lower coverage and 9.5 kJ/mol at higher methane coverage for H-CNT, indicating the physical nature for methane adsorption over open-tip CNTs.

1. Introduction

Methane (CH₄) produced by coal seam and shale is widely regarded as one of the main greenhouse gases contributing to global warming, which is one of the most significant challenges today [1–3]. The ongoing use of fossil fuels makes it compelling to store CH₄ via the adsorption technology. In recent decades, there has been an increasing interest to develop CH₄ storage systems for environmental purposes and energy applications [4, 5]. It is therefore highly desirable to develop adsorption materials with moderate adsorption capacity and good stability [6–10].

Structurally carbon materials, depending on their properties, can be used in CH₄ storage, due to their high specific surface area and pore volume that is able to host large amounts of CH₄ [2, 3, 11, 12]. More importantly, the textural property and surface chemistry of carbon materials for effectively increasing the amounts of stored gas can be appropriately tailored. Among the diverse adsorbents, CNTs

are considered to be one of the most promising candidates for CH₄ storage due to their low cost, high surface area, excellent thermal stability, and high amenability to pore structure tailoring [13–15]. However, CH₄ adsorption on the as-prepared CNTs is generally a weak physisorption process, which means that the uptake capacity can be low. A higher adsorption capacity in CH₄ storage of the open-tip CNTs than the as-prepared ones was obtained due to the larger specific surface area. Hence, it is necessary to open the tips of the as-grown CNTs before application. Generally, there are several approaches to achieve the purpose, such as strong acid oxidation and plasma treatment [16, 17]. There has been currently intensive research efforts focused on enhancing the adsorbate-adsorbent interaction and CH₄ storage via the increase of the specific surface area of adsorbents. One simple approach is to fabricate the adsorbents having increased surface area by HNO₃ modification [18].

In the present study, we investigated the open-tip effect of the as-prepared CNTs on their structure and adsorption

performance. The pristine CNTs was synthesized by CVD in a quartz tube reactor, and a series of open-tip carbon nanotubes (CNTs) were obtained by HNO₃ modification with various concentrations of as-prepared CNTs. The structural property was determined by N₂ adsorption/desorption at 77 K, scanning electron microscopy (SEM), X-ray diffraction (XRD), Raman spectroscopy, Fourier-transform infrared spectroscopy (FT-IR), and thermogravimetric analysis (TGA), respectively. The data of methane adsorption equilibrium were measured by a volumetric method, and experimental results of methane adsorption by CNTs were described by the model isotherms such as Langmuir and Dubinin–Astakhov (D-A) models. Furthermore, heat of adsorption was evaluated based on the Clausius–Clapeyron equation.

2. Experimental

2.1. Synthesis of the Adsorbents. The pristine CNTs was synthesized by CVD in a quartz tube reactor (inner diameter = 3.5 cm) laid in a horizontal furnace with a thermocouple in its central zone [19–21]. The catalyst loaded in a ceramic boat was reduced at 550°C in H₂ gas for 1 h and then raised to the reaction temperature of 650°C. Subsequently, the system was switched to methane of high purity (50 mL/min) for 1 h. After the reaction, the as-grown CNTs were cooled to room temperature in N₂ atmosphere. The product was collected and labeled as O-CNT.

2.1.1. Synthesis of L-CNTs. 3.0 g of O-CNTs was modified in 200 mL of 4.0 M HNO₃ refluxing at 110°C for 4 h. After cooling to room temperature, it was filtered and washed with deionized water until the pH of the filtrate was around 7. Finally, the product was dried at 60°C for 12 h and named as L-CNT.

2.1.2. Synthesis of M-CNTs. 3.0 g of O-CNTs was modified in 200 mL of 10.0 M HNO₃ refluxing at 110°C for 10 h. Others were similar to the above. Finally, the product was dried at 60°C for 12 h and represented by M-CNT.

2.1.3. Synthesis of H-CNTs. 3.0 g of O-CNTs was modified in 200 mL of 14.8 M (68 wt.%) HNO₃ refluxing at 110°C for 15 h. Others were similar to the above, and the sample was dried at 60°C for 12 h and denoted as H-CNT.

2.2. Characterization. The textural characterization of the samples was obtained by N₂ adsorption/desorption isotherms, determined at 77 K with a NOVA1000e surface area and pore size analyzer (Quantachrome Company) [19, 22]. The specific surface areas were determined according to the BET method. Total pore volume was calculated from the nitrogen volume held at $p/p_0 = 0.98\text{--}0.99$, and the micropore volume was estimated using the HK equation.

Surface morphology was investigated by scanning electron microscopy (SEM) (Hitachi S-4800, Japan).

X-ray diffraction of the samples was recorded in DX-1000 powder diffractometer equipped with Cu K α X-ray source and an internal standard of silicon powder.

Raman studies of the CNTs samples were conducted using a Renishaw inVia Raman spectrometer (UK) with an excitation source of 532 nm.

FT-IR analysis of the samples was performed on a Nicolet DXC20 FTIR spectrometer.

TGA of the samples was performed on a thermogravimetric analyzer (TGA Q500). The samples were heated at a rate of 10°C/min under N₂ atmosphere.

2.3. Methane Adsorption Evaluation. Methane adsorption isotherms were conducted using a volumetric method similar to that previously described [10, 13, 22]. Prior to each experiment, the samples were degassed for 3 h at 323 K, and after the samples were cooled down to the required temperature, helium was introduced into the system in order to calibrate the void volume in the adsorption setup via helium expansion. The purities of helium and methane were 99.999% and 99.99%, respectively. Methane adsorption test was operated under pressure ranges of 0–4.0 MPa at 298 K, and the adsorption process was repeated three times to guarantee the validity of the experimental data.

3. Results and Discussion

3.1. Textural and Structural Characteristics. The porosity parameters of the samples were studied by adsorption analysis using N₂ as the adsorbate molecule [1]. Figure 1 shows the N₂ adsorption/desorption isotherms at 77 K for the as-prepared CNTs and the corresponding open-tip samples. From the shapes and type of the obtained isotherms (type II of the IUPAC classification), it can be concluded that all the samples presented a micromesoporous character, for the isotherms displayed small hysteresis loops reflecting a minimum presence of mesopores. Furthermore, the HNO₃ modification process carried out provoked a continuous increase in the adsorption capacity of N₂. As exhibited in Figure 1, the volume amount adsorbed (cm³/g) increased with the increase of HNO₃ concentration.

Table 1 summarizes the textural characterization results for the pristine and modified adsorbents, as calculated from N₂ adsorption/desorption isotherms. The specific surface area for the pristine CNTs (O-CNT) was the lowest (98.7 m²/g) with a micropore volume of 0.0392 cm³/g which was less than half of the total pore volume (0.120 cm³/g). The modified CNTs suffered a drastic increase in all textural properties, indicating that HNO₃ may have opened the tips of the as-prepared sample. For the sample H-CNT modified with 14.8 M HNO₃ refluxing at 110°C for 15 h, a BET specific surface area of 174.4 m²/g and a HK micropore volume of 0.0682 cm³/g were reached.

To investigate the effect of HNO₃ modification with various concentrations and treating times on the modified CNTs, SEM observation was employed to obtain the morphology of the resulted samples. As shown in Figure 2, some

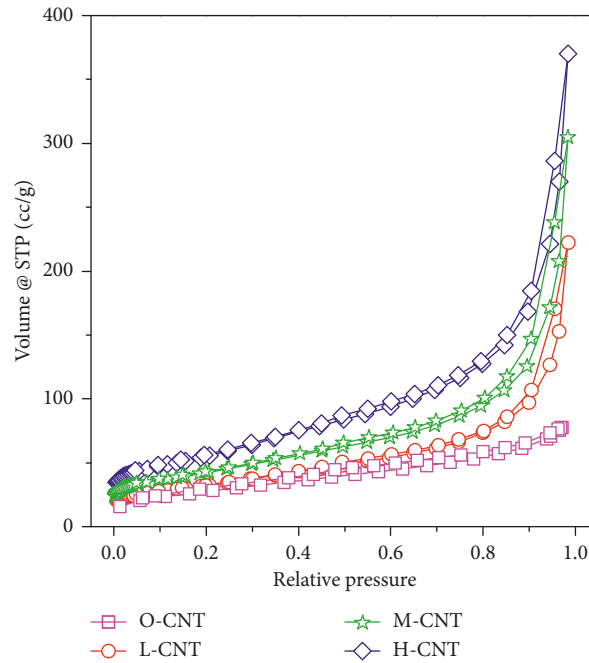


FIGURE 1: N_2 adsorption/desorption isotherms at 77 K corresponding to the samples.

TABLE 1: Textural characteristics obtained by N_2 adsorption analyses of the samples.

Sample	S_{BET} (m^2/g)	V_t (cm^3/g)	V_{HK} (cm^3/g)
O-CNT	98.7	0.120	0.0392
L-CNT	128.6	0.349	0.0495
M-CNT	150.2	0.471	0.0608
H-CNT	174.4	0.562	0.0682

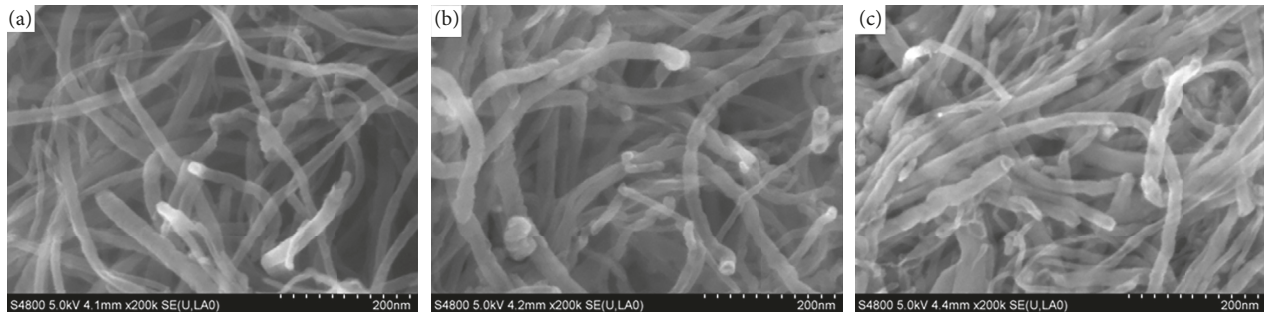


FIGURE 2: SEM images of L-CNT (a), M-CNT (b), and H-CNT (c).

tips of the modified CNTs were open, and the external diameter of CNTs was mainly distributed in the range of 10~34 nm, illustrating the carbon nanotubes were multi-walled. It could be seen that, in spite of various HNO_3 concentrations, the samples of L-CNT, M-CNT, and H-CNT presented no apparent difference in morphology. Comparatively, the H-CNT sample displayed a much larger amount of open-tip due to the accelerated activation process at higher HNO_3 concentration.

In order to study the influence of HNO_3 concentrations on crystalline phase, the X-ray diffraction (XRD) analysis

was conducted to characterize the structural property of the samples [23–26], and the results are shown in Figure 3. The (002) peak emerged at 26° , corresponding to the interplanar spacing of 0.34 nm. Also, the (100) peak at 43° was observed. Furthermore, the crystalline structure of the samples was not significantly altered by HNO_3 concentrations, suggesting the concentration of HNO_3 had no obvious effect on the structural property of the modified CNTs.

Raman spectra of the samples, shown in Figure 4, presented a prominent D-band (defects) at 1350 cm^{-1} and a G-band at 1575 cm^{-1} . The increase of the G-band relative

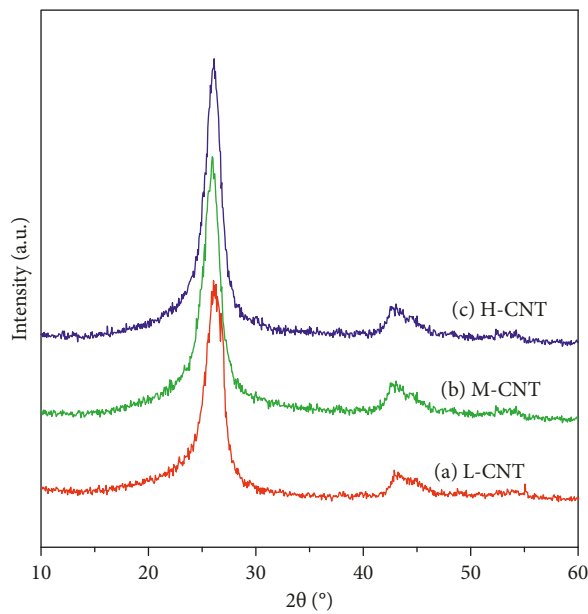


FIGURE 3: XRD patterns of the samples.

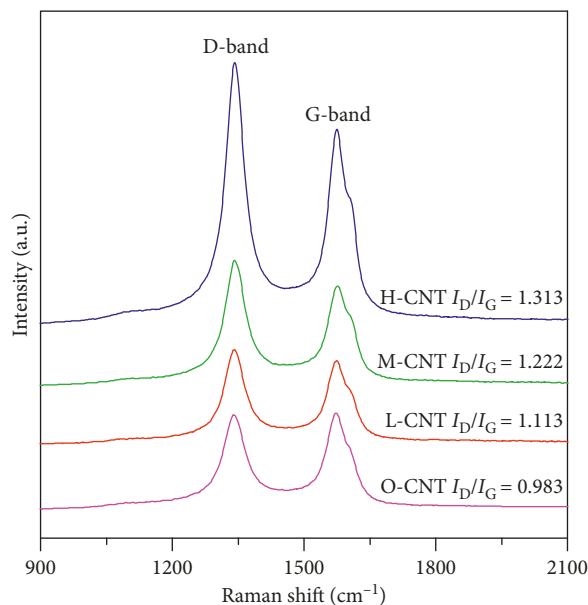


FIGURE 4: Raman spectra of the CNT samples.

intensity indicated an improvement of the crystallite orientation; however, the increasing D-band relative intensity suggested more defects and an increasing amount of disordered structure. The pertinent Raman parameter I_D/I_G , mentioned to account for the degree of structural order, as displayed in Figure 4, confirmed the structure development of the samples (I_D/I_G values of O-CNT, L-CNT, M-CNT, and H-CNT were 0.983, 1.113, 1.222, and 1.313, respectively). The HNO_3 oxidation of CNTs opened the tube tips, and according to the results of Raman spectra, HNO_3 modification can produce some structural defects in addition to eliminating tube ends.

FT-IR profiles for the modified CNTs are displayed in Figure 5. The samples exhibited similar FT-IR spectra, suggesting that they had similar structures and functional groups. A strong absorption band appeared at around 3400 cm^{-1} which was assigned to $-\text{OH}$ stretching. The adsorption peaks observed at $2900\text{ cm}^{-1}\sim 3000\text{ cm}^{-1}$ and $1670\text{ cm}^{-1}\sim 1760\text{ cm}^{-1}$ were attributed to $-\text{COOH}$ group vibrations. The peak appearing at $1000\text{ cm}^{-1}\sim 1200\text{ cm}^{-1}$ can be attributed to esters, such as those in ethers, phenols, and hydroxyl groups. However, all those peaks were more pronounced in H-CNT, suggesting the presence of more oxygen functional groups.

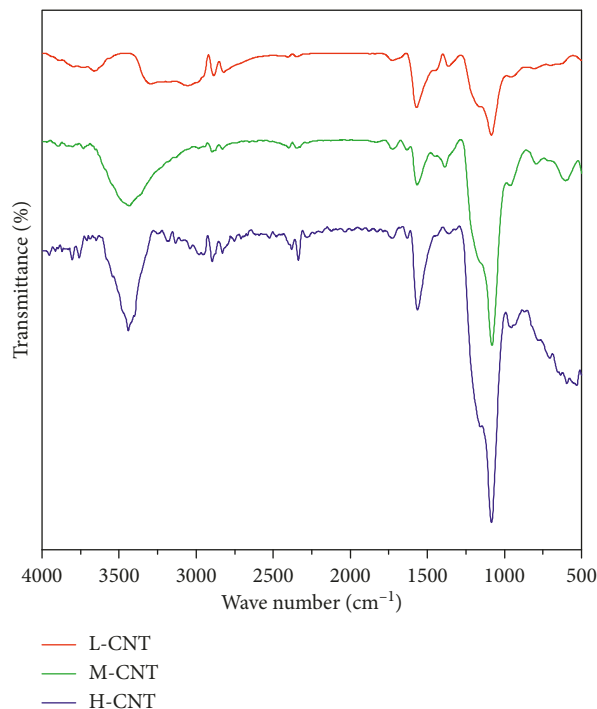


FIGURE 5: FT-IR spectra for the samples.

Thermogravimetric analysis (TGA) measured from room temperature to 800°C at N₂ atmosphere with a heating rate of 10°C/min has been used to study the structural changes for the samples modified by HNO₃ modification with various concentrations [27]. The initial sample weight was measured at room temperature. As confirmed in Figure 6, the weight loss for H-CNT (13.62%) due to oxygen functional groups was generally higher than those for other CNTs (9.45% for L-CNT and 12.36% for M-CNT), which was consistent with the FT-IR results.

3.2. Methane Adsorption Performance. The CH₄ adsorption data measured at 298 K and up to 4.0 MPa on the CNT samples are displayed in Figure 7. It was noteworthy that the H-CNT sample exhibited a higher CH₄ uptake due to its higher surface area and abundant micropores, followed by M-CNT and L-CNT, and the sample O-CNT had the smallest adsorption capacity among all the prepared adsorbents. The CH₄ adsorption isotherms were type I of IUPAC and described by Langmuir and Dubinin–Astakhov (D-A) models, respectively. The corresponding adsorption parameters of the models are given in Tables 2 and 3, and it can be concluded that the D-A model fitted the data better than the Langmuir model, for the mean relative deviation δ for D-A model was smaller than that for Langmuir model.

The parameter t in the D-A model describes the surface heterogeneity. It has been reported that the surface of the adsorbent is less heterogeneous when the t value is approaching 3 more ($t < 3$). Table 3 shows the value of t decreased with the modification concentration increasing. The higher the HNO₃ concentration was, the more

heterogeneous the sample was, which ultimately led to a greater CH₄ uptake.

It is well known that the methane adsorption is a physical process, mainly dependent on the specific surface area and micropore volume (shown in Figure 8). The relationship between n_0 (from the D-A model) and BET specific surface area (BET SSA) is presented in Figure 8. The result showed BET SSA was roughly proportional to n_0 and the correlation coefficient R^2 was 0.962. Also, the relationship between n_0 and micropore volume is exhibited in Figure 8, and the correlation coefficient R^2 was 0.989, which was higher than that for BET SSA. This was because the micropore volume not specific surface area was a more important factor for gas adsorption on carbon materials.

Figure 9 shows the heat of adsorption H_{ads} as a function of surface loading (n/n_0). As shown in Figure 9, the H_{ads} varied largely with the surface loading for all the samples, and it lay in the range of 9.5~19.4 kJ/mol, indicating the physical nature of the adsorption process. Due to the surface heterogeneity of the adsorbents and the stronger interaction between the CNTs and methane, the H_{ads} decreased with surface loading increasing. However, when n/n_0 approached above 0.75, the H_{ads} of the O-CNT, L-CNT, and M-CNT increased to a little higher value, indicating that the interaction between the adsorbent and methane was weaker and methane/methane interactions within the adsorption layer became obvious.

4. Conclusions

To investigate the structural features of open-tip CNTs for the methane adsorption capacity, the as-prepared CNTs synthesized via the CVD method were treated by HNO₃

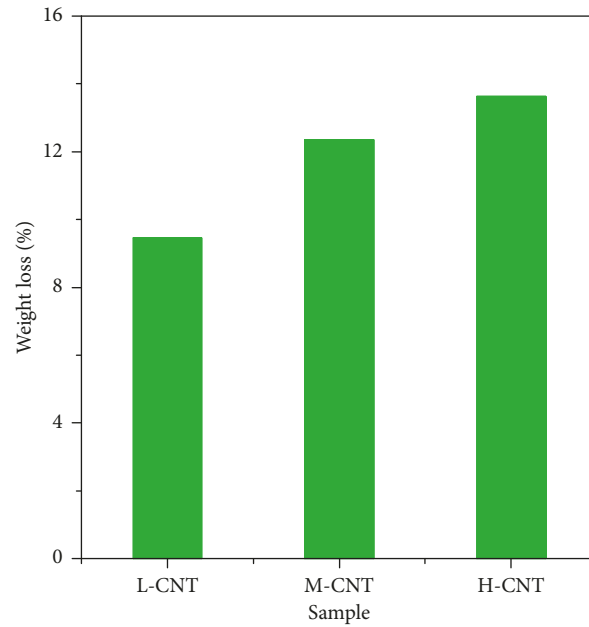


FIGURE 6: Weight loss of the modified CNTs under N_2 atmosphere.

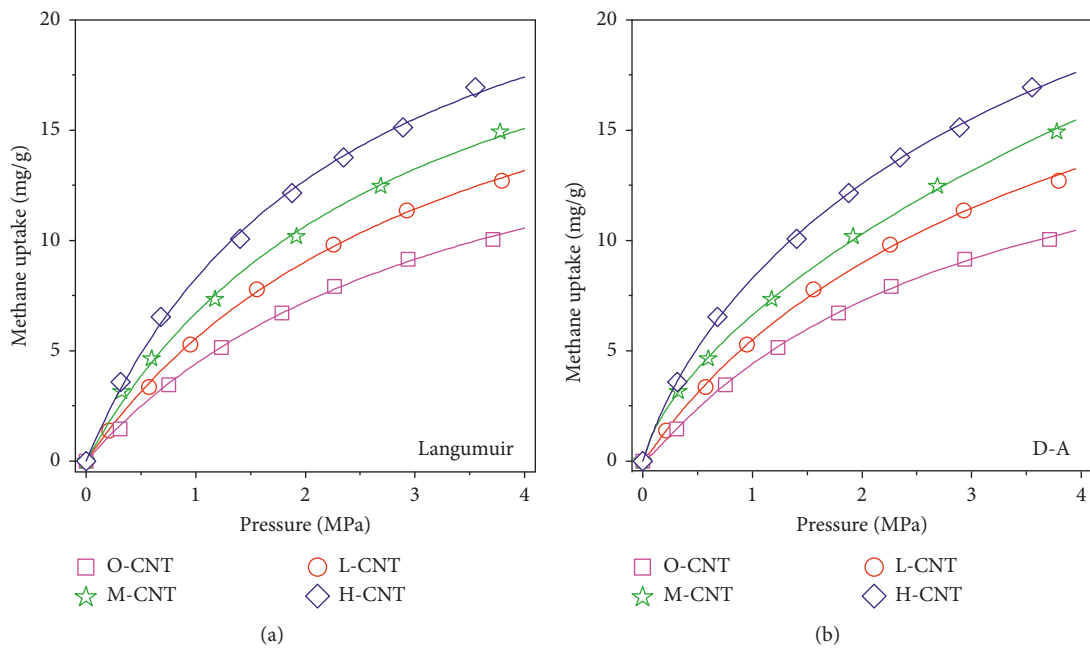


FIGURE 7: Equilibrium isotherms of methane adsorption on the samples at 298 K: (a) Langmuir model; (b) D-A model.

TABLE 2: Langmuir parameters of equilibrium isotherms for methane adsorption.

Sample	Mean relative deviation δ (%)	n_L (mg/g)	b (MPa^{-1})
O-CNT	3.88	19.75	0.287
L-CNT	2.27	24.23	0.297
M-CNT	6.06	25.84	0.350
H-CNT	3.79	27.55	0.429

TABLE 3: Adsorption parameters of the D-A model for methane adsorption isotherms.

D-A model	O-CNT	L-CNT	M-CNT	H-CNT
n_0 (mg/g)	13.62	18.55	24.00	26.15
E (kJ/mol)	5.59	5.27	5.75	5.55
t	1.73	1.53	1.47	1.15
Mean relative deviation δ (%)	0.68	1.75	1.02	1.01

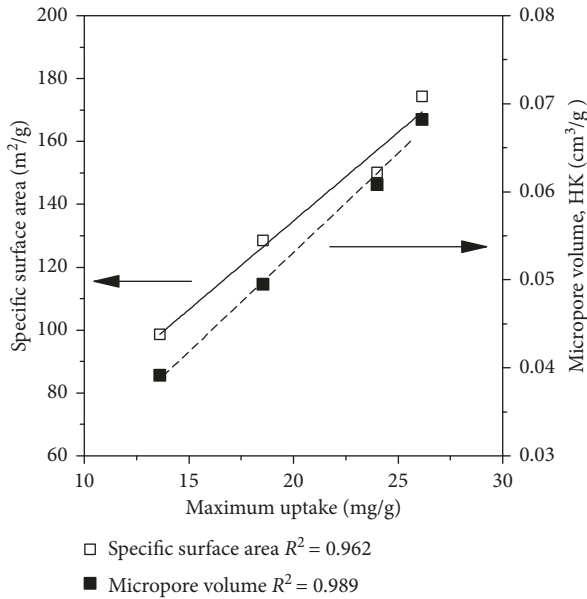


FIGURE 8: Maximum adsorption capacity (D-A model) related to BET specific surface area and micropore volume.

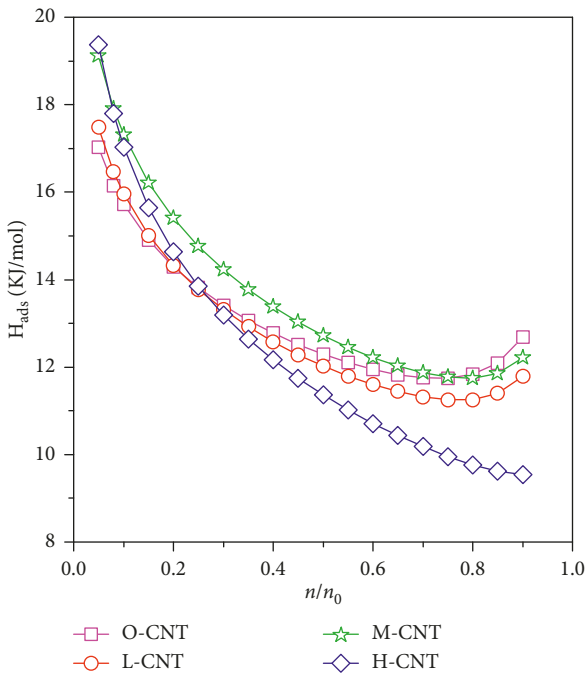


FIGURE 9: Heat of adsorption (H_{ads}) against different surface loadings (n/n_0) at 298 K.

modification with various concentrations. The modified CNTs had higher specific surface area, larger total pore volume, and greater micropore volume than those of the as-prepared CNTs. Such unique structural features allowed remarkably high methane uptakes, which was an effective way to improve the adsorption capacity when compared with the original CNTs. The resultant H-CNT exhibited high methane uptake of 26.15 mg/g from the D-A model, which was nearly as twice as the uptake of original CNTs (13.62 mg/g). The heat of adsorption was initially 19.4 kJ/mol at lower coverage and 9.5 kJ/mol at higher methane coverage for H-CNT, indicating the physical nature of methane adsorption over open-tip CNTs. The current study may have an impact on the advance of CNTs for practical application of CH_4 storage.

Data Availability

The data used to support the findings of this study are available from the corresponding author upon request.

Conflicts of Interest

The authors declare that they have no conflicts of interest.

Acknowledgments

This work was supported by the National Natural Science Foundation of China (Grant no. 21606058), the Natural Science Foundation of Guangxi (2017GXNSFBA198193 and 2017GXNSFBA198124), the Special Funding for Distinguished Expert from Guangxi Zhuang Autonomous Region, and the Startup Foundation for Doctors of Guilin University of Technology (no. 002401003510).

References

- [1] N. P. Wickramaratne and M. Jaroniec, "Activated carbon spheres for CO_2 adsorption," *ACS Applied Materials & Interfaces*, vol. 5, no. 5, pp. 1849–1855, 2013.
- [2] D. P. Bezerra, R. S. Oliveira, R. S. Vieira, C. L. Cavalcante Jr., and D. C. Azevedo, "Adsorption of CO_2 on nitrogen-enriched activated carbon and zeolite 13X," *Adsorption*, vol. 17, no. 1, pp. 235–246, 2011.
- [3] J. Marco-Lozar, M. Kunowsky, F. Suárez-García, J. Carruthers, and A. Linares-Solano, "Activated carbon monoliths for gas storage at room temperature," *Energy & Environmental Science*, vol. 5, no. 12, pp. 9833–9842, 2012.
- [4] Y. Lin, C. Kong, Q. Zhang, and L. Chen, "Metal-organic frameworks for carbon dioxide capture and methane storage," *Advanced Energy Materials*, vol. 7, no. 4, article 1601296, 2017.
- [5] Q. Chen, M. Luo, P. Hammershoj et al., "Microporous polycarbazole with high specific surface area for gas storage and separation," *Journal of the American Chemical Society*, vol. 134, no. 14, pp. 6084–6087, 2012.
- [6] Z. W. Zhu and Q. R. Zheng, "Methane adsorption on the graphene sheets, activated carbon and carbon black," *Applied Thermal Engineering*, vol. 108, pp. 605–613, 2016.
- [7] P. Arab, M. G. Rabbani, A. K. Sekizkardes, T. Islamoglu, and H. M. El-Kaderi, "Copper (I)-catalyzed synthesis of nanoporous azo-linked polymers: impact of textural properties on

- gas storage and selective carbon dioxide capture,” *Chemistry of Materials*, vol. 26, no. 3, pp. 1385–1392, 2014.
- [8] S. Cavenati, C. A. Grande, and A. E. Rodrigues, “Adsorption equilibrium of methane, carbon dioxide, and nitrogen on zeolite 13X at high pressures,” *Journal of Chemical & Engineering Data*, vol. 49, no. 4, pp. 1095–1101, 2004.
- [9] W. Zhou, H. Wu, M. R. Hartman, and T. Yildirim, “Hydrogen and methane adsorption in metal-organic frameworks: a high-pressure volumetric study,” *Journal of Physical Chemistry C*, vol. 111, no. 44, pp. 16131–16137, 2007.
- [10] Y. Y. Feng, W. Yang, N. Wang, W. Chu, and D. J. Liu, “Effect of nitrogen-containing groups on methane adsorption behaviors of carbon spheres,” *Journal of Analytical and Applied Pyrolysis*, vol. 107, pp. 204–210, 2014.
- [11] S. J. Yang, T. Kim, J. H. Im et al., “MOF-derived hierarchically porous carbon with exceptional porosity and hydrogen storage capacity,” *Chemistry of Materials*, vol. 24, no. 3, pp. 464–470, 2012.
- [12] Y. Xia, R. Mokaya, G. S. Walker, and Y. Zhu, “Superior CO₂ adsorption capacity on N-doped, high-surface-area, microporous carbons templated from zeolite,” *Advanced Energy Materials*, vol. 1, no. 4, pp. 678–683, 2011.
- [13] Y. Y. Feng, W. Yang, W. Chu, and C. F. Jiang, “Powdered multi-walled carbon nanotubes synthesized from various activated carbon-supported catalysts and their methane storage performance,” *Nanoscience and Nanotechnology Letters*, vol. 6, no. 10, pp. 875–880, 2014.
- [14] H. Tanaka, M. El-Merraoui, W. Steele, and K. Kaneko, “Methane adsorption on single-walled carbon nanotube: a density functional theory model,” *Chemical Physics Letters*, vol. 352, no. 5-6, pp. 334–341, 2002.
- [15] J. W. Lee, H. C. Kang, W. G. Shim, C. Kim, and H. Moon, “Methane adsorption on multi-walled carbon nanotube at (303.15, 313.15, and 323.15) K,” *Journal of Chemical & Engineering Data*, vol. 51, no. 3, pp. 963–967, 2006.
- [16] M. Ran, Y. Liu, W. Chu, and A. Borgna, “Enhanced conversion of cellobiose to sugar alcohols by controlled dispersion of ruthenium nanoparticles inside carbon nanotube channels,” *Catalysis Letters*, vol. 143, no. 11, pp. 1139–1144, 2013.
- [17] P. A. Denis, “Methane adsorption inside and outside pristine and N-doped single wall carbon nanotubes,” *Chemical Physics*, vol. 353, pp. 79–86, 2008.
- [18] S. Talapatra and A. Migone, “Adsorption of methane on bundles of closed-ended single-wall carbon nanotubes,” *Physical Review B*, vol. 65, no. 4, article 045416, 2002.
- [19] Y. Y. Feng, W. Yang, and W. Chu, “A study of CO₂ methanation over Ni-based catalysts supported by CNTs with various textural characteristics,” *International Journal of Chemical Engineering*, vol. 2015, Article ID 795386, 7 pages, 2015.
- [20] X. Pan, Z. Fan, W. Chen, Y. Ding, H. Luo, and X. Bao, “Enhanced ethanol production inside carbon-nanotube reactors containing catalytic particles,” *Nature Materials*, vol. 6, no. 7, pp. 507–511, 2007.
- [21] W. Yang, W. Chu, C. F. Jiang, J. Wen, and W. J. Sun, “Cerium oxide promoted Ni/MgO catalyst for the synthesis of multi-walled carbon nanotubes,” *Chinese Journal of Catalysis*, vol. 32, no. 6–8, pp. 1323–1328, 2011.
- [22] S. Hao, W. Chu, Q. Jiang, and X. P. Yu, “Methane adsorption characteristics on coal surface above critical temperature through Dubinin-Astakhov model and Langmuir model,” *Colloids and Surfaces A: Physicochemical and Engineering Aspects*, vol. 444, pp. 104–113, 2014.
- [23] H. Yusa and T. Watanuki, “X-ray diffraction of multiwalled carbon nanotube under high pressure: structural durability on static compression,” *Carbon*, vol. 43, no. 3, pp. 519–523, 2005.
- [24] A. Cao, C. Xu, J. Liang, D. Wu, and B. Wei, “X-ray diffraction characterization on the alignment degree of carbon nanotubes,” *Chemical Physics Letters*, vol. 344, no. 1-2, pp. 13–17, 2001.
- [25] C. Müller, D. Golberg, A. Leonhardt, S. Hampel, and B. Büchner, “Growth studies, TEM and XRD investigations of iron-filled carbon nanotubes,” *Physica Status Solidi (A)*, vol. 203, no. 6, pp. 1064–1068, 2006.
- [26] R. A. Ismail, M. I. Mohammed, and L. H. Mahmood, “Preparation of multi-walled carbon nanotubes/n-Si heterojunction photodetector by arc discharge technique,” *Optik*, vol. 164, pp. 395–401, 2018.
- [27] D. Qian, C. Lei, G. P. Hao, W. C. Li, and A. H. Lu, “Synthesis of hierarchical porous carbon monoliths with incorporated metal-organic frameworks for enhancing volumetric based CO₂ capture capability,” *ACS Applied Materials & Interfaces*, vol. 4, no. 11, pp. 6125–6132, 2012.

